A Design Model for Electric Environmental Control System in Aircraft Conceptual and Preliminary Design

Praise Worthy Prize

This paper is available online at www.praiseworthyprize.org
International Review of Aerospace Engineering (I.RE.AS.E), Vol. 16, N. 2
ISSN 1973-7459 *April 2023*

A Design Model for Electric Environmental Control System in Aircraft Conceptual and Preliminary Design

M. Fioriti, F. Di Fede

Abstract – *In present decades, the need for a more efficient air transport system is driving towards more electric aircraft subsystems. Electrified subsystems offer the opportunity to optimize the operational performance of systems by reducing the power required by the propulsion system therefore, reducing the fuel burnt. A considerable advantage can be obtained by electrifying the environmental control system which is the most power demanding aircraft subsystem. The paper presents a simplified model to estimate the main performances of the conventional and electrified environmental control system during the aircraft conceptual and preliminary design phases. Different air cycle machine architectures can be designed. The model is divided in two main modules. The first is dedicated to the estimation of the aircraft thermal loads including the effect of solar radiation, the conduction of external air, the presence of passengers and the avionic systems. With the main result of estimating the cabin airflow required to control the temperature and the air quality within the aircraft's mission profile. The second module of the model designs all major components of the air conditioning pack including the dedicated compressors of the electrified environmental control system. The model requires basic input data that can be easily estimated during the early stages of aircraft design. The model is calibrated using the available data of a conventional system and then applied to the electrified one. The results show the increased efficiency of the electrified system that results from optimizing both pneumatic power generation and the air cycle machine.* ***Copyright © 2023 The Authors.***

Keywords: *Air Cycle Machine, Cabin Thermal Loads, Environmental Control System, More Electric Aircraft, Systems Electrification*

Nomenclature

A_{he}	Heat transfer area of the heat exchanger [m^2]
$A_{windows}$	Total area of transparent surfaces [m^2]
ACM	Air Cycle Machine
ACP	Air Conditioning Pack
BP	Bypass duct
BPV	Bypass Valve
C	Centrifugal compressor
C_{ACM}	ACM compressor
C_E	E-ECS dedicated compressor
c_p	Specific heat of air at constant pressure [J/(kg K)]
$c_{p,5}$	Specific heat at constant pressure of the air entering the condenser [J/(kg K)]
$c_{p,6}$	Specific heat at constant pressure of the air exiting the condenser [J/(kg K)]
$c_{p,condenser}$	Mean value of the specific heat at constant pressure of the air in the condenser [J/(kg K)]
C_{max}	Maximum heat capacity rate [W/s]
C_{min}	Minimum heat capacity rate [W/s]
COND	Condenser
COND LP	Low pressure duct of the condenser
COND HP	High pressure duct of the condenser
CV	Check Valve
ECS	Environmental Control System
E-ECS	Electric-Environmental Control System
f_r	Recovery factor
f_{rad}	Windows radiation factor
FCV	Flow Control Valve
FL	Flight Level
G_{sun}	Solar radiation [W/m^2]
h_2'	Specific enthalpy of the air passing through the by-pass valve [J/kg]
h_5	Specific enthalpy before condensation [J/kg]
h_6	Specific enthalpy after condensation [J/kg]
h_7	Specific enthalpy of the air after expansion in ACM turbine [J/kg]
h_8	Specific enthalpy of the air exiting MIX 1 [J/kg]
k_i	Thermal conductivity of the layer [W/(m K)]
I	Air intake
ISA	International Standard Atmosphere
l_{cabin}	Cabin length [m]

Available online by April 30th, 2023 https://doi.org/10.15866/irease.v16i2.23379

l_f	Fuselage length [m]
LCD	Liquid Crystal Display
M	Electric motor
M_0	Mach number of the air entering the air intake
$\dot{m}_{ACM}$	Air mass flow passing through the air cycle machine [kg/s]
$\dot{m}_{BP}$	Air mass flow passing through the by-pass valve [kg/s]
$\dot{m}_{ECS}$	Air mass flow provided by the air conditioning system [kg/s]
MIX 1	First mixer
MIX 2	Second mixer
N_{aisle}	Number of light strips in the corridor
N_{crew}	Number of crew members
N_{floor}	Number of light strips on the cabin floor
N_{pax}	Number of passengers
NTU	Number of Transfer Units
OPV	Over Pressure Valve
p_0	Outside air static pressure [Pa]
p_1^0	Total air pressure exiting the air intake [Pa]
p_a^0	Total pressure of the air exiting the fan [Pa]
p_{ram}^0	Total pressure of the air entering in the fan inlet [Pa]
P_{air}	Pneumatic power of the flow processed by the fan [W]
$P_{avionics}$	Electric power required by the avionic system [W]
$P_{aisle\ light}$	Electrical power required by the aisle light strip [W/m]
P_c	Power of the dedicated compressor [W]
$P_{c,ACM}$	Power of the ACM compressor [W]
$P_{display}$	Electrical power required by the single display [W]
$P_{floor\ light}$	Electrical power required by the light strip of the floor [W/m]
P_{motor}	Power of the electric motor that drive the dedicated compressor [W]
Pr	Prandtl number
$P_{reading\ light}$	Electric power required by a single reading light [W]
$P_{t,ACM}$	Power of the ACM turbine [W]
PHE	Primary Heat Exchanger
$\dot{q}_{avionics}$	Heat flow due to the avionic system [W]
$\dot{q}_{cond}$	Heat flow due to the fuselage thermal conductivity [W]
$\dot{q}_{condenser}$	Total heat flow exchanged in the condenser [W]
$\dot{q}_{conv,int}$	Heat flow due to internal convention [W]
$\dot{q}_{crew}$	Heat flow due to the crew [W]
$\dot{q}_{display}$	Heat flow due to the displays [W]
$\dot{q}_{he}$	Heat flow in the heat exchanger [W]
$\dot{q}_{lat}$	Latent heat in the condenser [W]
$\dot{q}_{lights}$	Heat flow due to the lights system [W]
$\dot{q}_{met}$	Heat flow due to the metabolic heat dissipated from occupant [W]
$\dot{q}_{pax}$	Heat flow due to the passengers [W]
$\dot{q}_{rad,Earth}$	Heat flow due to the Earth radiation [W]
$\dot{q}_{rad\ transp\ sur}$	Heat flow due to the solar radiation throughout transparent surfaces [W]
$\dot{q}_{rad,sky}$	Heat flow due to the sky radiation [W]
$\dot{q}_{rad,Sun}$	Heat flow due to the solar radiation [W]
$\dot{q}_{sen}$	Sensible heat in the condenser [W]
$\dot{q}_{tot}$	Total heat flow throughout the fuselage [W]
$\dot{Q}_{fan}$	Volumetric flow rate processed by the fan [m^3/s]
$r_{avionics}$	Ratio between avionic thermal load and avionic electric power [1/m^2]
R_{fus}	Fuselage thermal resistance [K/W]
r_i	Internal radius of the i-th layer [m]
r_{i+1}	External radius of the i-th layer [m]
r_{light}	Ratio between lighting system thermal load and lighting system electric power [1/m^2]
RHE	Reheater
SFC	Specific Fuel Consumption
SHE	Secondary Heat Exchanger
T	Turbine
T_0	Outside static air temperature [K]
T_1^0	Total temperature of the air exiting the air intake [K]
T_2	Air temperature of the primary flow entering in the PHE [K]
T_3	Air temperature of the primary flow exiting from the PHE [K]
T_4	Temperature of the air exiting the ACM compressor [K]
T_5	Temperature of the air exiting from the SHE [K]
T_6	Temperature of the air entering the ACM turbine [K]
T_7	Temperature of the air after expansion in ACM turbine [K]
T_{ACM}	ACM turbine
T_b	Air temperature of the secondary flow entering the PHE [K]
T_c	Air temperature of the secondary flow exiting from the PHE [K]
T_{cab}	Desired cabin air temperature [K]
T_{ECS}	Temperature of the air leaving the conditioning system [K]
T_r	Recovery temperature [K]
T_{SA}	Static external air temperature [K]
$T_{skin,ext}$	External skin temperature [K]
$T_{skin,int}$	Internal skin temperature [K]
U_{he}	Overall heat transfer coefficient of the heat exchanger [J/(m^2 K s)]
β_c	Pressure ratio of the dedicated compressor
$\beta_{c,ACM}$	Pressure ratio of the ACM compressor
$\beta_{t,ACM}$	Pressure ratio of the ACM turbine
γ	Heat capacity ratio of the air
Δp_{fan}^0	Increase in air total pressure due to the fan [Pa]
ε_{ai}	Efficiency of the air intake
η_{fan}	Efficiency of the fan

$\eta_{is,c}$	Isentropic efficiency of the dedicated compressor
$\eta_{is,c,ACM}$	Isentropic efficiency of the ACM compressor
$\eta_{is,t,ACM}$	Isentropic efficiency of the ACM turbine
η_{mec}	Dedicated compressor mechanical efficiency
$\eta_{mec,c}$	Mechanical efficiency of the ACM compressor
$\eta_{mec,f}$	Mechanical efficiency of the secondary flow fan
$\eta_{mec,t}$	Mechanical efficiency of the ACM turbine
η_{motor}	Electric motor efficiency
τ	Coefficient of transmissivity of glass

I. Introduction

The Environmental Control System (ECS) is the most power demanding system of a passenger transport aircraft [1]-[3]. The ECS provides fresh, pressurized air to the aircraft's passengers and crew throughout the flight. The air supplied by the ECS should have a precise temperature in order to cool or heat the cabin air within a comfortable temperature range. The conventional ECS is powered by the pneumatic system which distributes part of the pneumatic power produced by the engine compressors. The temperature and pressure of the air produced by the propulsion system strongly depends on the engine power settings. The maximum values are reached during takeoff and climb phases when the engine speed is close to the maximum power. However, the power required by ECS is independent of the engine power settings and derives from both the passengers' needs and the external environmental conditions (e.g., air temperature and pressure, humidity, and solar radiation).

Usually, the ECS requires a significant amount of power even when the engine is in idle state or at low power settings. In particular, when the aircraft is on ground in hot day conditions or during descent. Therefore, the traditional pneumatic system and ECS are usually oversized during the other phases of the mission when the engine is in climb and cruise ratings [4]. This produces some inefficiencies, as part of the extra pneumatic power supplied by the engine has to be wasted to supply the ECS with the right amount of power, or more exactly, with air having lower pressure and temperature than that supplied by the engine [2], [5].

Additionally, propulsion system efficiency decreases when aircraft systems require pneumatic or mechanical power. It is worth noting that the effect of bleeding the air from engine compressors is more detrimental to engine efficiency than the mechanical power extracted from the engine shaft [6]-[8]. Since the effect of power extraction is an increase in engine Specific Fuel Consumption (SFC), this effect extends to total propulsive power which is more than an order of magnitude greater than the power required by the aircraft systems alone. For these reasons, in the last decades, an Electric Environmental Control System (E-ECS) has been proposed and employed in Boeing 787 [9]. This is one of several new technologies involved in aircraft electrification such as high voltage generation and distribution, electric anti-ice, and electric actuators. [2], [10]-[14]. The E-ECS is supposed to increase the efficiency of the system by producing the necessary pneumatic power itself. In this case, the pneumatic power is no longer provided by engine compressors, but it is produced by dedicated compressors driven by electric motors [9], [15]. Therefore, the E-ECS is disconnected from the bleed air system and from the influence of the engine power settings. Dedicated compressors can produce the exact amount of pneumatic power required by ECS, at each phase of the mission, while saving fuel.

Furthermore, having the possibility to better controlling the pressure and temperature of the air supplied to the ECS, it is possible to optimize the ECS itself by increasing its efficiency during cruise condition. More details are provided in Section III.2. The present paper presents a complete E-ECS model to estimate the cabin heat loads and the power required by the E-ECS within the main aircraft mission phases. The model designs all the main equipment of the system, and it is also compatible with conventional ECS. During the aircraft conceptual and preliminary design phases, the model is particularly useful to perform specific trade off studies on systems architectures (e.g., air cycle machine with different number of wheels) and to estimate the greater part of the secondary power (i.e., the power needed by the aircraft subsystems) required during flight.

Despite the relatively high detail level of the results obtainable from the proposed model, the number of inputs is limited, and they can already be known during the first phases of aircraft design. Most of the models in the literature are focused on the conventional ECS [16]-[20] or some of its specific components such as heat exchangers [21], [22] and air cycle machines [23], [24].

A small part of the literature models deals with E-ECS (e.g. [25], [22], [26] but they require detailed input data available only in the later design phases. For instance, these models require the geometry of the heat exchangers, the characteristics of the main system valves and the diameter and length of the secondary flow duct.

Other models are developed to perform system optimization [27], [28] or system health management [23], [24] rather than ECS design. Most models focus on analyzing only one or two design points, usually cruise or ground conditions. The model here presented can design the ECS considering a more complete operating flight envelope since multiple points could require specific performance that contribute to ECS sizing. For instance, hot ground conditions are essential to design for maximum cooling performance, cold ground and flight conditions are required to determine the maximum heating performance and pressurization requirement. The model is based on the following multiple design points:

- Hot ground conditions: aircraft stationary on the ground, sunny and hot day conditions (ISA+25);
- Cold ground conditions: aircraft stationary on the

ground, cold day conditions (ISA-35);
- Flight conditions: aircraft on cruise (ISA-20).

Differently from some other models that focus on the dynamic behavior of specific ECS components [22], [19], [20], [29], the proposed model calculates the main operating parameters for the system design. In this way, the model defines the static air flow, temperatures, and pressures of each main system component. This reduces the complexity of the analysis allowing a complete study and system sizing. Finally, compared to the other models, the present one adds external air humidity as parameters to correctly design the system when operating in hot ground conditions. The model is composed of two modules:
- Cabin thermal loads and required ECS air mass flow estimation;
- Environmental control system performance estimation and E-ECS pneumatic power generation.

The first module is divided into two sub-parts. The first, described in section II.1, considers the different thermal loads to which the cabin is exposed. Therefore, it estimates the thermal loads due to passengers, solar radiation, internal lights, and equipment. The thermal load due to the conduction when the aircraft is moving through the air is also considered. The second part, described in II.2, estimates the required airflow at a specific temperature and pressure to cool or heat the cabin. The second module is in turn divided into two parts. The first (Section II.3) performs the design of the specific E-ECS components needed to produce the pneumatic power. The second part, described in sections II.4, is dedicated to the performance of the E-ECS and considers the main components of the E-ECS such as primary and secondary heat exchangers, pressure reduction and shut off valve, air cycle machine, and water separator. The result is the power required by the system to pressurize and condition the cabin air.

Eventually, in Section III, two test cases are presented to calibrate and to confirm the accuracy of the model.

II. ECS and E-ECS Model Description

For a better understanding of the model operation, a general block diagram of the whole model architecture is shown in Fig. 1. The model requires some general information about aircraft data, mission profile, Air Conditioning Pack (ACP) configuration, temperature limit for the cabin air and for the air coming from the vents. Firstly, the data is used to calculate the fuselage heat load for the different mission profile phases. Starting from the heat load, the model estimates the air mass flow (supplied by the ACP) needed to balance the heat load at a cabin temperature included in the range required by the regulation. Initially, the model designs the ACP to use the lowest allowable temperature for the air from the vents when the objective is to cool the cabin (or the highest allowable temperature when the objective is to heat the cabin). This increases system efficiency by reducing the ACP air flow.

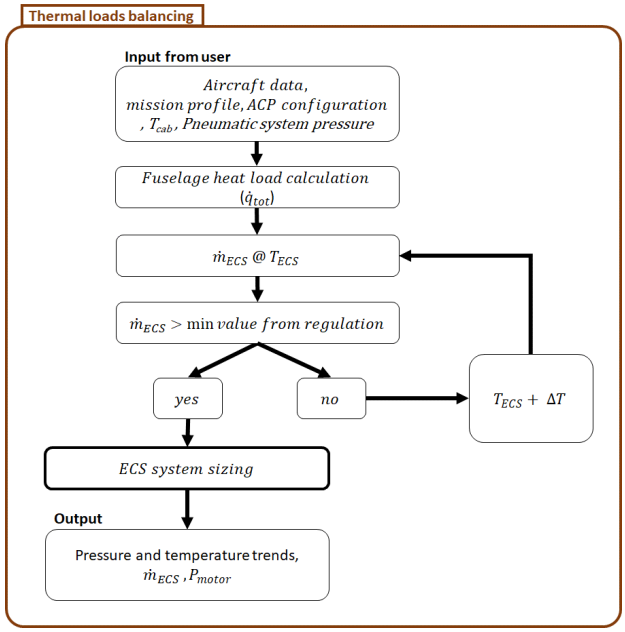

Fig. 1. General block diagram of the ECS/E-ECS model

However, as shown in Fig. 1, the model checks the air flow value to ensure this value is greater than the minimum fresh air required by the regulation. If the air flow is not compliant, the temperature of the air from the air vents is increased (or decreased) until the requirement is satisfied. For each iteration, the ACP is re-designed accordingly. At the end of the design process, the output module is reported. In particular, the model provides the characteristics of the air (i.e. air flow, temperature, pressure etc.) in each ECS component and evaluates its power budget for each phase of the mission profile.

II.1. Fuselage Heat Load Calculation

The calculation of the cabin heat load represents the starting point of the ECS design. Cabin heat load balancing is one of the main system performance requirements. The total heat load consists of several contributions:
- Metabolic heat flow dissipated by the occupants ($\dot{q}_{met}$);
- Equipment heat flow dissipated by the avionics ($\dot{q}_{avionics}$), display ($\dot{q}_{display}$) and cabin lights ($\dot{q}_{lights}$);
- Heat flow due to fuselage thermal conductivity ($\dot{q}_{cond}$);
- Heat flow due to solar radiation through transparent surfaces (i.e. passengers' windows and windscreens) ($\dot{q}_{rad\ transp\ sur}$).

The total heat flow through the fuselage is given by Equation (1):

$$\dot{q}_{tot} = \dot{q}_{met} + \dot{q}_{avionics} + \dot{q}_{display} + \\ + \dot{q}_{lights} + \dot{q}_{cond} + \dot{q}_{rad\ transp\ sur} \quad [\mathrm{W}] \tag{1}$$

Each fuselage heat flow contributor is analyzed below.

II.1.1. Metabolic Heat Flow

The human body regulates its temperature by exchanging heat with the environment, this means that the human body is a sensitive and latent heat source. The heat load produced by human beings depends on age, the cabin air temperature and the activities they are carrying out. The Equation (2) [30] is usually used to calculate the heat load produced by passengers and crew:

$$\dot{q}_{met} = \dot{q}_{crew} \cdot N_{crew} + \dot{q}_{pax} \cdot N_{pax} \quad [W] \qquad (2)$$

where $\dot{q}_{crew} = 130$ W is the typical value for the metabolic heat generated by the crew, N_{crew} is the number of crew members, $\dot{q}_{pax} = 70$ W is the typical value for the metabolic heat generated by the passengers, N_{pax} is the number of passengers.

II.1.2. Avionics, Displays and Lights Heat Loads

Electronic equipment is one of the most important heat sources. There are different types of electrical equipment installed onboard a civil transport aircraft. In addition to the avionic equipment, the aircraft is equipped with devices needed to provide passengers' comfort. The electrical equipment, distributed through the aircraft (e.g., lights, passenger displays, etc.), exchange heat directly with the cabin. Conversely, the avionic equipment is normally installed in one or more dedicated compartments called avionics bays. Usually, the air coming from the cabin is used to cool down the equipment in the avionic bay. Depending on aircraft design, if the air used to cool the avionics is expelled from the aircraft, the avionic heat loads do not contribute to the total heat load. The heat load generated by avionics corresponds to the required electrical power reduced by a coefficient $r_{avionics}$ (Equation (3)):

$$\dot{q}_{avionics} = r_{avionics} \times P_{avionics} \quad [W] \qquad (3)$$

where $P_{avionics}$ is the avionics electric power [W], $r_{avionics} = 0.95$ is the typical value of the ratio between the avionic thermal load and the avionic electrical power.

The coefficient $r_{avionic}$ considers the electric power that is not converted into heat and, therefore, does not contribute to the heat load, such as the power emitted by the aircraft antennas. The displays are an important part of the onboard entertainment system and, usually, their quantity is equivalent to the total number of cabin seats.

The heat load generated by the displays can be calculated with Equation (4):

$$\dot{q}_{display} = (N_{pax} + N_{cabin\,crew}) \times P_{display} \quad [W] \qquad (4)$$

where N_{crew} is the number of cabin crew members, N_{pax} is the number of passengers, $P_{display}$ is the electrical power consumption by a single display [W]. The electrical power required by a display depends on the size and on the screen technology. For example, the electrical power required by a 9-inch LCD screen is about 8.4 W. The heat flow produced by the internal lighting system should also be considered. Reading lights for passengers and cabin crew, floor lighting for escape routes and aisle lighting must be calculated. As for the avionic system, a coefficient (r_{light}) to convert the electric power of the lighting system into heat is needed.

Additionally, to calculate the heat produced by the cabin lights, the cabin length is needed. Since during the first phase of the aircraft design this information could be little known, a ratio between the cabin and fuselage length may be used. It is usually between 0.65 and 0.75:

$$\dot{q}_{lights} = r_{light}\big[(N_{pax} + N_{crew})P_{reading\ light} + \\ + \frac{l_{cabin}}{l_f} \times l_f\big(P_{floor\ ligth} \times N_{floor} + \\ + P_{aisle\ light} \times N_{aisle}\big)\big] \quad [W] \qquad (5)$$

where r_{ligth} is the ratio between lighting system thermal load and lighting system electric power, N_{pax} is the number of passengers, N_{crew} is the number of cabin crew members, $P_{reading\ light}$ is the electric power required by a single reading light [W], l_f is the fuselage length [m], l_{cabin} is the cabin length lighted up by the lighting system [m], $P_{floor\ light}$ is the electrical power required by the light strip of the floor [W/m], $P_{aisle\ light}$ is the electrical power required by the aisle light strip [W/m], N_{floor} is the number of light strips on the cabin floor, N_{aisle} is the number of light strips in the aisle.

II.1.3. Fuselage Heat Flow due to Thermal Conduction

To evaluate the heat flow due to thermal conduction, the fuselage of the aircraft can be outlined in the three following layers (as depicted in Fig. 2):

- Layer n. 1 – Internal skin: it is usually made of composite material or plastic and it has a decorative function;
- Layer n. 2 – Insulating/structural layer: in the central layer there are structural elements, electrical cables, ducts, and a layer of insulating material. To evaluate the thermal flow, the intermediate layer is considered homogeneous having the thermal characteristics of the insulating layer. One of the insulating materials widely used in aeronautics is the microlite with thicknesses ranging from 25 mm to 51 mm [26];
- Layer n. 3 – External skin: the external coating is made of aluminum or composite material, and it has the function of supporting aerodynamic and structural loads.

The heat flow due to conduction through the fuselage skin can be calculated with Equation (6):

$$\dot{q}_{cond} = \frac{T_{skin,ext} - T_{skin,int}}{R_{fus}} \quad [W] \qquad (6)$$

where $T_{skin,ext}$ is the external skin temperature [K], $T_{skin,int}$ is the internal skin temperature [K], R_{fus} is the fuselage thermal resistance [K/W].

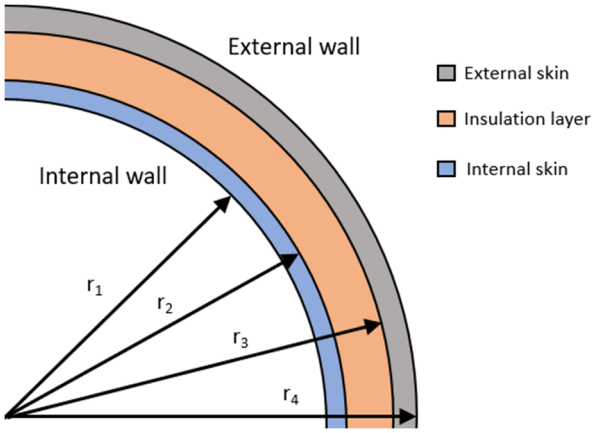

Fig. 2. The main three layers of the fuselage

Since the fuselage has a multilayer cylindrical geometry, the thermal resistance of the fuselage is given by the relationship (7) [31]:

$$R_{fus} = \sum_{i=1}^{3} R_i = \sum_{i=1}^{3} \frac{\log\left(\frac{r_{i+1}}{r_i}\right)}{2\pi(l_{cabin})k_i} \quad [\text{K/W}] \qquad (7)$$

where R_i is the thermal resistance of the i-th layer [K/W] r_i is the internal radius of the i-th layer [m], r_{i+1} is the external radius of the i-th layer [m], l_{cabin} is the cabin length [m], k_i is the thermal conductivity of the layer [W/(m K)]. Thermal conductivity is a measure of a substance's ability to transmit heat. Table I shows the thermal conductivity of the most common material for each fuselage layer.

When the aircraft is on ground, it is necessary to solve the following system of non-linear equations in the unknowns $T_{skin,int}$ and $T_{skin,est}$ to calculate the temperatures of the internal and external fuselage walls:

$$\begin{cases} \dot{q}_{conv,int} = \dot{q}_{cond} \\ \dot{q}_{rad,Sun} + \dot{q}_{rad,Earth} + \dot{q}_{rad,sky} + \\ +\dot{q}_{conv,est} = \dot{q}_{cond} \end{cases} \qquad (8)$$

where $\dot{q}_{conv,int}$ is the heat flow due to internal convention [W], $\dot{q}_{cond}$ is the heat flow due to the fuselage thermal conductivity [W], $\dot{q}_{rad,Sun}$ is the heat flow due to the solar radiation [W], $\dot{q}_{rad,Earth}$ is the heat flow due to the Earth radiation [W], $\dot{q}_{rad,sky}$ is the heat flow due to the sky radiation [W], $\dot{q}_{conv,esxt}$ is the heat flow due to the external convention [W]. Fig. 3 shows the equivalent electric circuit [26], [31] of the fuselage thermal resistance.

TABLE I
THERMAL CONDUCTIVITY OF THE MOST COMMON MATERIAL FOR EACH FUSELAGE LAYER

Material	Thermal conductivity [W/(m K)]
Aluminum	205
Microlite (insulating)	0,04
Composite (carbon fibers)	0,3

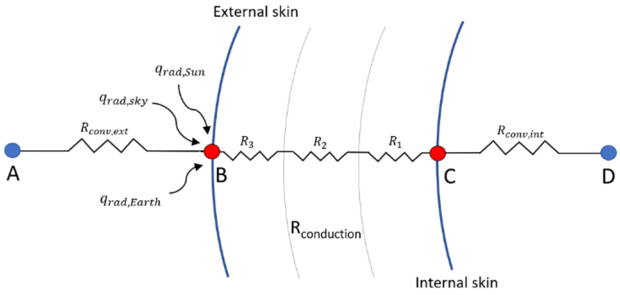

Fig. 3. Equivalent electric circuit of the fuselage thermal resistance

The first equation of the system is given by the heat flow balance in node C, while the second equation represents the flow balance in node B. Nodes A and D represent respectively the external stationary conditions defined by the standard atmosphere model and the desired cabin conditions. For the sake of brevity, the detailed calculation of $T_{skin,ext}$ and $T_{skin,int}$ is not here explained. Interested readers will find the full description in [30]. When the aircraft is in flight, the external wall temperature is assumed to be equal to the recovery temperature T_r as prescribed in [32]:

$$T_{skin,est} = T_r = T_{amb}\left(1 + f_r\frac{\gamma - 1}{2}M^2\right) \quad [\text{K}] \qquad (9)$$

$$f_r = \sqrt[3]{Pr} \qquad (10)$$

where T_{SA} is the static external air temperature [K], $f_r = \sqrt[3]{Pr}$ is the recovery factor, Pr is the Prandtl number, M is the Mach number, γ is the heat capacity ratio of the air. In flight conditions, to calculate the thermal flux through the opaque surfaces of the fuselage it is sufficient to solve the balance at node C since the temperature of the external wall is known.

II.1.4. Fuselage Heat Flow due to Solar Radiation Through the Windows

Solar radiation transfers energy to the fuselage external skin and into the fuselage through the windows. The effect on the fuselage external skin is already considered in the external skin temperature and thermal conduction. The heat flow due to solar radiation through transparent surfaces can be calculated with the following relationship:

$$\dot{q}_{rad\ transp\ sur} = \tau G_{sun} f_{rad} A_{windows} \quad [\text{W}] \qquad (11)$$

where τ is the coefficient of transmissivity of glass, G_{sun} is the solar radiation [W/m^2], f_{rad} is the windows radiation factor, $A_{windows}$ is the total area of transparent surfaces [m^2]. The windows radiation factor has been defined to consider that solar radiation cannot directly penetrate through all fuselage windows at the same time.

It is usually a number close to 0.5.

II.2. Assessment of the ECS Air Mass Flow

To balance the total fuselage heat load $\dot{q}_{tot}$, the air conditioning system must provide a certain amount of air mass flow $\dot{m}_{ECS}$ which can be calculated with the relationship (12):

$$\dot{m}_{ECS} = \frac{\dot{q}_{tot}}{c_p(T_{ECS} - T_{cab})} \quad [\text{kg/s}] \qquad (12)$$

where $\dot{q}_{tot}$ is the total fuselage heat load [W], c_p is the specific heat of air at constant pressure [J/(K kg)], T_{ECS} is the temperature of the air leaving the conditioning system [K], T_{cab} is the desired cabin air temperature [K].

II.3. Pneumatic Power Generation

As far as conventional ECS is concerned, the pneumatic power is usually generated by the propulsion system through the bleed system. Therefore, a small part of the compressed air is extracted from the engine compressors and used to supply the ECS and other pneumatic users. Since the engine power rating changes during the flight, the compressed air is usually taken from low-pressure or high-pressure ports depending on the engine rating. In this way, the two bleed ports attempt to provide a uniform range of pneumatic power. When the engine is operated at the idle rating, the high-pressure port is used. Conversely, the low-pressure port is used when the engine is operated at climb, cruise or full rating.

However, the pneumatic utilities, such as the ECS, require pneumatic power according to their specific needs. For this reason, the pneumatic system of a conventional aircraft is provided with a heat exchanger (i.e. pre-cooler) and a throttling valve to regulate the air temperature and pressure dissipating the extra pneumatic power. For more electric aircraft, such as the Boeing 787, pneumatic power is generated using one or more centrifugal compressors driven by electric motors. This eliminates the need of bleed air from the engine using dedicated compressors with variable speed to generate the exact amount of pneumatic power required. The control of the electric motors allows an optimization of the energy consumption since, unlike the conventional system, the pressure is no longer regulated with the throttling valves with consequent loss of energy but with the motor speed. The airflow of the environmental control system can be regulated according to the number of people aboard the aircraft to obtain the least energy consumption in compliance with the requirements imposed by the regulations [30], [32]. A simple schematic of the electric pneumatic power generation system is shown in Fig. 4. For safety reasons, the system has two lanes connected to each Air Conditioning Pack (ACP) and the two lanes are connected using an X-valve. Each lane consists of an air intake (I), centrifugal dedicated compressor (C), electric motor (M), Over Pressure Valve (OPV) and a Check Valve (CV). Each ACP can be isolated using the pack valve.

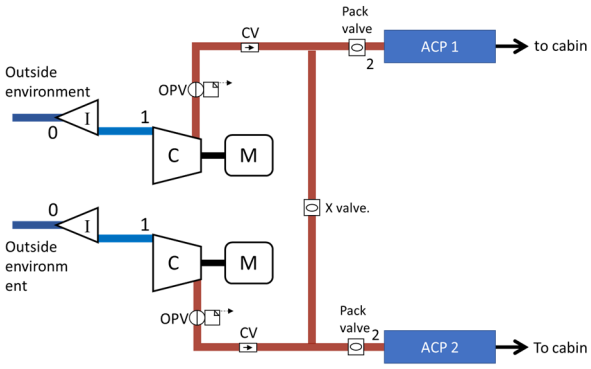

Fig. 4. E-ECS Pneumatic power generation

II.3.1. Air Intake

The air intake is designed to provide the flow required by the air conditioning and pressurization system while generating the minimum aerodynamic drag. The airflow passing through the air intake decreases its speed and consequently increases its pressure. To calculate the performance of the air intake, the following assumptions are made:

- The capture section is equal to the entrance section: in this way the cruising Mach coincides with the Mach of the air entering the intake and the presence of the fuselage is neglected;
- The outflow is almost static, therefore, the air temperature and pressure conditions correspond to the stagnation conditions;
- Adiabatic compression.

Under these assumptions, given the external air conditions (T_0, p_0) and the flight Mach M_0, it is possible to calculate the total temperature T_1^0 and the total pressure p_1^0 exiting the air intake:

$$T_1^0 = T_0\left(1 + \frac{\gamma - 1}{2}M_0^2\right) \quad [\text{K}] \qquad (13)$$

$$p_1^0 = \varepsilon_{ai} p_0 \left(\frac{T_1^0}{T_0}\right)^{\frac{\gamma}{\gamma-1}} \quad [\text{Pa}] \qquad (14)$$

where T_0 is the outside air static temperature [K], M_0 is the Mach number, p_0 is the outside air static pressure [Pa], $\varepsilon_{ai} = p_1^0/p_0^0$ is the efficiency of the air intake.

When the aircraft is stationary on the ground, ε_{ai} is equal to 1 since there is no total pressure loss.

II.3.2. Motor-Driven Compressor

Adiabatic compression formulas are used to size the compressor. The compressor power P_c can be obtained from Equation (15):

$$P_c = \frac{\dot{m}_{ECS} c_p T_1^0}{\eta_{is,c}}\left[\beta_c^{\frac{\gamma-1}{\gamma}} - 1\right] \quad [\text{W}] \qquad (15)$$

where T_1^0 is the total temperature of the air exiting the air

intake [K], $\eta_{is,c}$: isentropic efficiency of the dedicated compressor, β_c is the pressure ratio of the dedicated compressor. In particular, the higher pneumatic power demand between cooling and heating conditions is considered the compressor sizing point:

- In cooling condition, the compressor supply air with suitable pressure and flow rate to the ACP so that the ACP provides cold air to the cabin;
- In heating condition, the compressor has to compress and heat the air to balance the cabin heat load.

In both cases, cabin pressurization and the minimum fresh air must be guaranteed. However, for centrifugal compressor, $\dot{m}_c$, β_c and $\eta_{is,c}$ are mutually dependent.

Therefore, the compressor operating point must be verified using a centrifugal compressor characteristic Fig. 5. The compressor map is developed by interpolating the typical operating points of a generic centrifugal compressor with a fourth-degree polynomial ($R^2 = 0.9914$). The compressor is driven by the electric motor which provides mechanical power. The electric motor power P_{motor} corresponds to the compressor power corrected with efficiency, which takes into account the mechanical losses and the efficiency of the electric motor:

$$P_{motor} = \frac{P_c}{\eta_{motor}\eta_{mec}} \quad [W] \tag{16}$$

where η_{mec} is the compressor mechanical efficiency, η_{motor} is the electric motor efficiency.

II.4. Thermodynamic Model of the ACP

Depending on aircraft category, cost and production year, the ECS uses different types of ACM. The proposed model considers the following types of ACM that cover the greater part of present aircraft:

- Two-wheel subfreezing bootstrap (shown in Fig. 6): this type of ACM consists of a compressor (C) and a turbine (T) connected together by means of a transmission shaft. The secondary flow is energized by a fan which is usually driven by a dedicated electric motor (M);
- Three-wheel subfreezing bootstrap (shown in Fig. 7): compared to the two-wheel bootstrap, the secondary flow fan has been added to the transmission shaft connecting the ACM turbine and compressor. In this way, the electric motor is removed. Using this architecture, the turbine supplies energy to both the compressor and the fan. The advantages are given by weight reduction. For this configuration, however, the rotational speeds are the same for all the components. Therefore, the system may not be fully optimized;
- Four-wheel subfreezing bootstrap (shown in Fig. 8): the ACM is equipped with two turbines. In this way, expansion occurs more gradually, increasing its efficiency. The drawback of this architecture is the increase in the overall system dimensions and complexity.

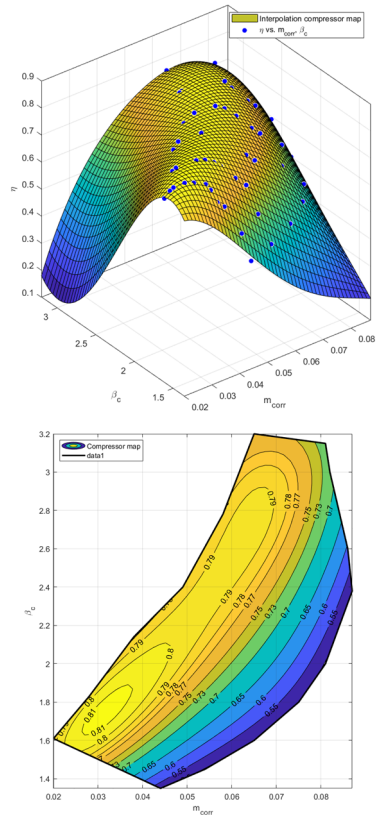

Fig. 5. Centrifugal compressor characteristics

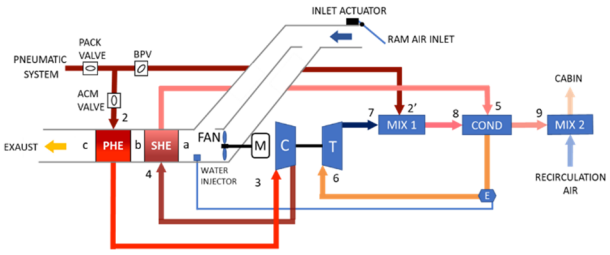

Fig. 6. Two-wheel subfreezing bootstrap ACP

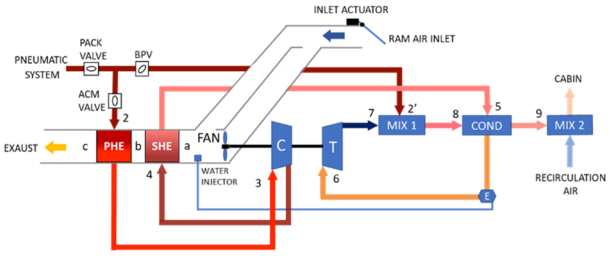

Fig. 7. Three-wheel subfreezing bootstrap ACP

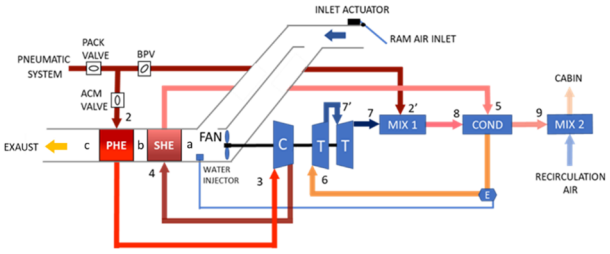

Fig. 8. Four-wheel subfreezing bootstrap ACP

To correctly evaluate the pneumatic power required by the ECS, all main ACP components have to be thermodynamically modelled. They are the Primary Heat Exchanger (PHE), the Secondary Heat Exchanger (SHE), ACM compressor, ACM turbine, condenser (COND), the first mixer (MIX 1), the second mixer (MIX 2), and the fan of the secondary flow. For a better understanding of how the proposed mathematical model of the ACP works, a more detailed block diagram is depicted in Fig. 9. The block diagram refers to the architecture of the e-ECS system as it is more complete than the conventional architecture. Due to the non-linearity of the system, the model is based on multiple convergence loops nested together. The outermost loops are required to determine the ACU supply pressure and flow rate of the secondary flow. The intermediate loop, on the other hand, allows to determine the correct air temperature of the secondary flow between the two heat exchangers. Finally, the internal loop is necessary to ensure the power balance to the ACM shaft. All the temperatures and pressures described in the following subsections are to be understood as total temperatures and total pressures.

II.4.1. Heat Exchanger

The following model can be applied to both PHE and SHE. In both cases, the fluids involved in the heat exchange process are the primary flow (i.e. the air flow delivered into the cabin) and the secondary flow (i.e. external flow needed to cool the ACP heat exchangers).

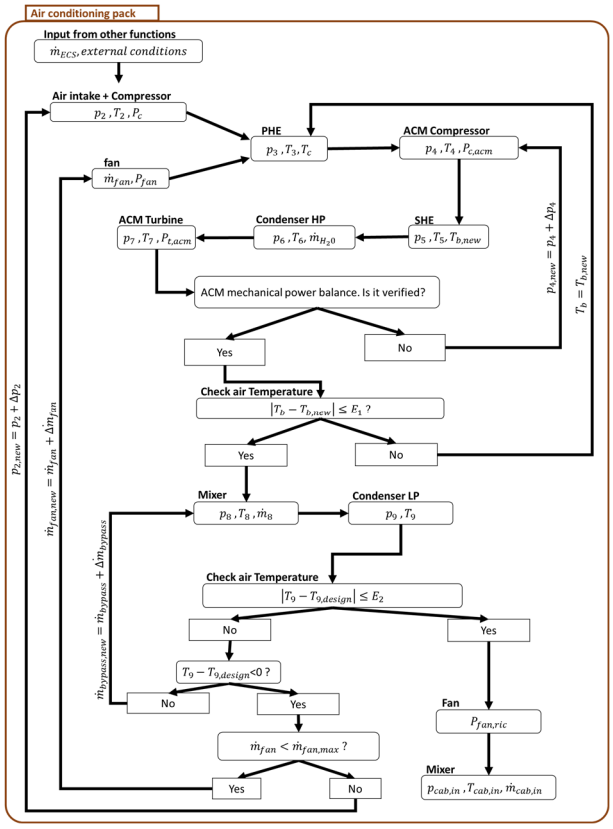

Fig. 9. Flowchart of the ACP model

With reference to the PHE and Fig. 8 (but also Fig. 6 and Fig. 7), the thermal power is calculated with the equation:

$$\dot{q}_{he} = \epsilon_{he} C_{min} |T_2 - T_b| \quad [\text{W}] \tag{17}$$

$$C_{\min} = \min\left\{(\dot{m}c_p)_2, (\dot{m}c_p)_b\right\} \quad [\text{W/s}] \tag{18}$$

where $\dot{q}_{he}$ is the heat flow in the heat exchanger [W], ϵ_{he} is the effectiveness of the heat exchanger, C_{min} is the minimum heat capacity rate [W/s], T_2 is the air temperature of the primary flow entering in the PHE [K], T_b is the air temperature of the secondary flow entering the PHE [K].

Applying the number of transfer units (NTU) [33], as can be seen from Fig. 10, the effectiveness of the heat exchanger is a function of the capacity rate ratio $\left(\frac{C_{min}}{C_{max}}\right)$ and NTU:

$$NTU = \frac{A_{he} U_{he}}{C_{min}} \tag{19}$$

where U_{he} is the overall heat transfer coefficient of the heat exchanger [J/(m^2 K s)], A_{he} is the heat transfer area of the heat exchanger [m^2].

Knowing the heat exchanger effectiveness, it is possible to determine the output temperatures of the flows:

$$\begin{aligned} T_3 &= T_2 \pm \frac{\dot{q}_{he}}{(\dot{m}c_p)_2} \quad [\text{K}] \\ T_c &= T_b \mp \frac{\dot{q}_{he}}{(\dot{m}c_p)_b} \quad [\text{K}] \end{aligned} \tag{20}$$

where T_3 is the air temperature of the primary flow exiting from the PHE [K], T_c is the air temperature of the secondary flow exiting from the PHE [K].

In the proposed model, the same mathematical model is applied and specialized also for the SHE.

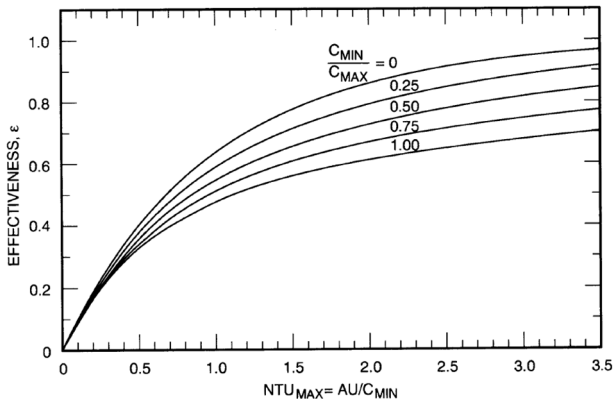

Fig. 10. Effectiveness versus NTU for various capacity rate ratios of cross flow heat exchanger [34]

II.4.2. ACM Compressor

The temperature of the air exiting from the ACM compressor T_4 is given by the following relationship:

$$T_4 = T_3\left[1 + \frac{1}{\eta_{is,c,ACM}}\left(\beta_{c,ACM}^{\frac{\gamma-1}{\gamma}} - 1\right)\right] \quad [\text{K}] \quad (21)$$

where $\beta_{c,ACM}$ is the pressure ratio of the ACM compressor, $\eta_{is,c,ACM}$ is the isentropic efficiency of the ACM compressor. Knowing the temperature increase due to the compression, it is possible to calculate the compressor power $P_{c,ACM}$:

$$P_{c,ACM} = \dot{m}_{ACM} c_p (T_4 - T_3) \quad [\text{W}] \quad (22)$$

where $\dot{m}_{ACM}$ is the air mass flow passing through the air cycle machine [kg/s].

II.4.3. ACM Turbine

The temperature of the air after the expansion in the turbine T_7 and the power of the turbine $P_{t,ACM}$ can be obtained from the following relationships:

$$T_7 = T_6\left[1 - \eta_{is,t,ACM}\left(1 - \frac{1}{\beta_{t,ACM}^{\frac{\gamma-1}{\gamma}}}\right)\right] \quad [\text{K}] \quad (23)$$

$$P_{t,ACM} = \dot{m}_{ACM} c_p (T_6 - T_7) \quad [\text{W}] \quad (24)$$

where T_6 is the temperature of the air entering the ACM turbine [K], $\beta_{t,ACM}$ is the pressure ratio of the ACM turbine, $\eta_{is,t,ACM}$ is the isentropic efficiency of the ACM turbine. When a four-wheel bootstrap ACP (Fig. 8) is selected, a better $\eta_{is,t,ACM}$ is considered to simulate the double turbine stage without complicating the model.

II.4.4. Condenser

The condenser removes the humidity of the primary airflow to avoid ice formation in the turbine. In this way, the optimal psychometric conditions are reached allowing condensation of the water vapor contained in the air.

Condensed water is thus eliminated with a water separator located downstream of the condenser. The total heat flow exchanged in the condenser $\dot{q}_{condenser}$ is defined by:

$$\dot{q}_{condenser} = \dot{q}_{sen} + \dot{q}_{lat} \quad [W] \quad (25)$$

where $\dot{q}_{sen}$ is the sensible heat in the condenser [W], $\dot{q}_{lat}$ is the latent heat in the condenser [W]. Analyzing in detail the contributions of the equation, $\dot{q}_{sen}$ can be calculated with the following relationships:

$$\dot{q}_{sen} = \dot{m}_{ACM} c_{p,condenser} (T_5 - T_6) \quad [W] \quad (26)$$

$$c_{p,condenser} = \left(\frac{c_{p,5} + c_{p,6}}{2}\right)\left[\frac{\text{J}}{\text{kg K}}\right] \quad (27)$$

where $c_{p,condenser}$ is the mean specific heat at constant pressure of the air in the condenser [J(kg K)], $c_{p,5}$ is the specific heat at constant pressure of the air entering the condenser [J(kg K)], $c_{p,6}$ is the specific heat at constant pressure of the air exiting the condenser [J(kg K)], T_5 is the temperature of the air exiting from the SHE [K]. The latent heat $\dot{q}_{lat}$ due to the phase transition is:

$$\dot{q}_{lat} = \dot{m}_{ACM}(h_5 - h_6) \quad [W] \quad (28)$$

where h_5 is the specific enthalpy before condensation [J/kg], h_6 is the specific enthalpy after condensation [J/kg];

II.4.5. Mixer

The mixer is used to mix two streams of moist air without supplying energy from the outside (adiabatic mixing). By specializing the general equation of the mixer for MIX 1 (Fig. 6), the physical and psychometric characteristics of the output stream are determined by making mass and energy balances:

$$\begin{cases} \dot{m}_{ACM} + \dot{m}_{BP} = \dot{m}_{ECS} \\ \dot{m}_{ACM} h_7 + \dot{m}_{BP} h_{2'} = \dot{m}_{ECS} h_8 \end{cases} \quad (29)$$

where $\dot{m}_{BP}$ is the air mass flow passing through the by-pass valve [kg/s], h_7 is the specific enthalpy of the air after expansion in ACM turbine [J/kg], $h_{2'}$ is the specific enthalpy of the air passing through the by-pass valve [J/kg], h_8 is the specific enthalpy of the air exiting MIX 1 [J/kg]. The same system of equations can be employed and specialized to model MIX 2 (Fig. 6).

II.4.6. Fan

A fan is required to activate the secondary air flow to cool the PHE and the SHE (Fig. 6) especially during ground operation. A fan is an operating machine that transmits energy to the air to increase the total air pressure. The total pressure processed by a fan corresponds to the total pressure increase Δp_{fan}^0 of the flow between the inlet and outlet sections:

$$\Delta p_{fan}^0 = p_a^0 - p_{ram}^0 \quad [\text{Pa}] \quad (30)$$

where p_{ram}^0 is the total pressure of the air entering in the fan inlet [Pa], p_a^0 is the total pressure of the air exiting the fan [Pa]. It is possible to calculate the pneumatic power of the flow processed by the fan P_{air} with the following relationship:

$$P_{air} = \dot{Q}_{fan} \Delta p_{fan}^0 \quad [\text{W}] \quad (31)$$

where $\dot{Q}_{fan}$ is the volumetric flow rate processed by the

fan [m^3/s]. Ultimately, the fan power P_{fan} is calculated using the following equation:

$$P_{fan} = P_{air}\eta_{fan} \quad [\text{W}] \tag{32}$$

where η_{fan} is the fan efficiency. It is worth noting that P_{fan} is used differently depending on the ACP technology. For the three and four-wheel subfreezing bootstrap ACPs (Fig. 7 and Fig. 8), P_{fan} is part of the ACM shaft balancing equation as described in Section II.4.7. Conversely, P_{fan} is used to design an electric motor in case a two-wheel subfreezing bootstrap ACP (Fig. 6) is selected.

II.4.7. Mechanical Power Balance of ACM Shaft

Depending on the architecture of the ACM chosen, a different shaft power balance is performed. In particular, if the ACM is a two-wheel bootstrap:

$$P_{t,ACM}\,\eta_{mec,t} = \frac{P_{c,ACM}}{\eta_{mec,c}} \quad [\text{W}] \tag{33}$$

Conversely, for the three/four-wheel bootstrap ACM, the relationship (34) is used:

$$P_{t,ACM}\eta_{mec,t} = \frac{P_{c,ACM}}{\eta_{mec,c}} + \frac{P_{fan}}{\eta_{mec,f}} \quad [\text{W}] \tag{34}$$

where $P_{t,ACM}$ is the power of the ACM turbine [W], $\eta_{mec,t}$ is the mechanical efficiency of the ACM turbine, $P_{c,ACM}$ is the power of the ACM compressor [W], $\eta_{mec,c}$ is the mechanical efficiency of the ACM compressor, P_{fan} is the power of the secondary flow fan [W], $\eta_{mec,f}$ is the mechanical efficiency of the secondary flow fan.

III. Model Calibration and Validation

To calibrate the ECS model, assumptions regarding the thermodynamic coefficients and efficiencies of the ACP components are defined by comparing the model results with data of a conventional ECS reported in the ACP Training Manual of Liebherr Aerospace [35].

Subsequently, the calibrated model is applied to the Boing 787, the only civil aircraft that adopts E-ECS, to validate the proposed model with the available data.

III.1. Model Calibration

The available data [35] are mainly related to the air temperature values in the various components of the ACP of the A320-200 aircraft. Comparing the ACP architecture currently used in the A320-200 aircraft (i.e. three wheels) with the one modeled in the present work, it is worth noting that the main difference lies in the presence of the reheater (RHE), which is not considered in the proposed model for keep it as simple as possible.

However, RHE does not cause major changes in overall performance of the ACP, as the temperature changes experienced by the air in this heat exchanger are relatively modest. The general inputs for the proposed model are listed in Table II. They relate to the main specifications of the aircraft and the type of ACP. Known and estimated data of the A320 are considered here.

Three specific conditions are evaluated to calibrate the model:

- *Case 1:* cooling conditioning when aircraft is stationary on the ground on a hot day condition (ISA+25) with the maximum number of passengers and during daylight hours;
- *Case 2:* heating conditioning when aircraft is stationary on the ground on a cold day condition (ISA-35) with the minimum number of passengers and during night-time;
- *Case 3:* heating conditioning when aircraft is in flight (flight level 250) and on a cold day condition (ISA-20).

In Table III the detailed inputs are listed. They are mainly assumptions concerning the efficiency or pressure drops of the main component of the ACP.

TABLE II
GENERAL INPUT OF THE ECS MODEL FOR THE A320 AIRCRAFT

General input	Unit of measure	Value
Number of passenger	-	180
Number of crew members	-	6
Cruise Mach	-	0.78
Passenger window area	m^2	0.075
Cockpit window area	m^2	2.36
Fuselage length	m	37.57
Fuselage radius	m	1.97
Flag passenger monitor	-	yes
Thickness of the outer skin of the fuselage	m	0.002
Thermal conductivity of the outer skin of the fuselage	W/(m K)	0.3
Thickness of the insulating layer of the fuselage	m	0.035
Thermal conductivity of the insulating layer of the fuselage	W/(m K)	0.04
Thickness of the decorative layer of the fuselage	m	0.005
Thermal conductivity of the fuselage decorative layer	W/(m K)	0.3
Wheel number of the ACM	-	3
ACP subfreezing	-	yes
Minimum cabin pressure	bar	0.7562
Minimum air flow required per passenger	kg/s	0.0042

TABLE III
DETAIL INPUT OF THE ECS MODEL FOR THE A320 AIRCRAFT

Detail input	Unit of measure	hot day (ISA+25) ground	cold day (ISA-35) ground	cold day (ISA -20) FL250
Isentropic efficiency of the ACM compressor	-	0.77	0.7	0.75
Isentropic efficiency of the ACM turbine	-	0.8	0.7	0.75
Mechanical efficiency of the ACM	-	0.98	0.98	0.98
Fan Efficiency	-	0.68	0.68	0.68
Mechanical efficiency of the fan	-	0.95	0.95	0.95
Electric Motor Fan efficiency	-	0.93	0.93	0.93
Pressure losses of the ram air	Pa	6000	6000	6000
Pressure losses of the recirculation air	Pa	5000	5000	5000
Cabin air temperature	°C	27	21	21

The values of the air temperatures and pressures in the various components of the ACP are shown in Fig. 11, Fig. 12 and Fig. 13. The red stars depicted in the graphs represent the reference values (only temperatures are available) [35] used to calibrate the model. As can be seen from Fig. 11, Fig. 12, and Fig. 13, the proposed ECM model accurately estimates the values of the real air conditioning pack of the A320-200 aircraft. Some slight differences can be observed in the PHE in cold-ground conditions (Fig. 12) and in the COND HP in flight conditions (Fig. 13).

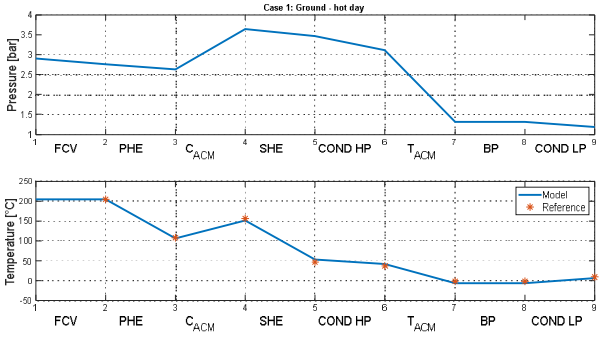

Fig. 11. Conventional ECS - ground hot day (where FCV = Flow Control Valve, PHE = Primary Heat Exchanger, C_{ACM} = ACM compressor, SHE = Secondary Heat Exchanger, COND HP = high pressure duct of the condenser, T_{ACM} = ACM turbine, BP = ByPass duct, COND LP = low pressure duct of the condenser)

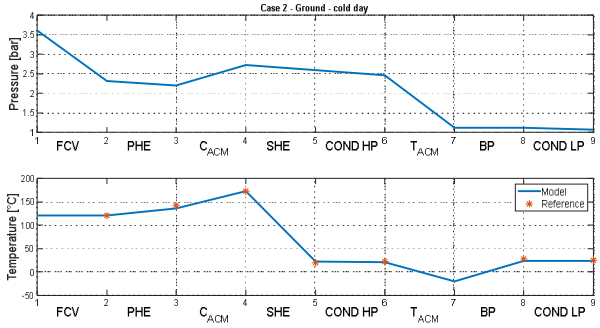

Fig. 12. Conventional ECS - ground cold day (where FCV = Flow Control Valve, PHE = Primary Heat Exchanger, C_{ACM} = ACM compressor, SHE = Secondary Heat Exchanger, COND HP = high pressure duct of the condenser, T_{ACM} = ACM turbine, BP = ByPass duct, COND LP = low pressure duct of the condenser)

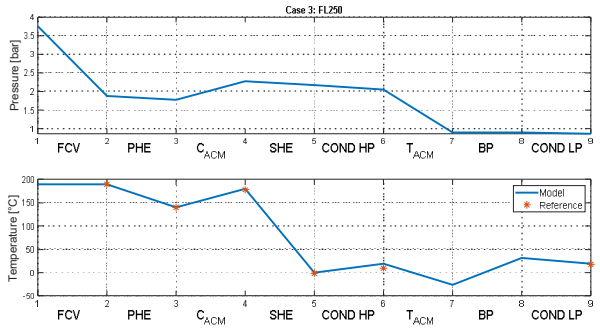

Fig. 13. Conventional ECS - FL250 cold day (where FCV = Flow Control Valve, PHE = Primary Heat Exchanger, C_{ACM} = ACM compressor, SHE = Secondary Heat Exchanger, COND HP = high pressure duct of the condenser, T_{ACM} = ACM turbine, BP = ByPass duct, COND LP = low pressure duct of the condenser)

III.2. Model Calibration and Validation

To validate the proposed model with the E-ECS system, the Boeing 787 Dreamliner is used as reference aircraft being the only commercial passenger airliner using that type of ECS. The general inputs of the aircraft are shown in Table IV. The same three design cases of the conventional ECS were examined. Furthermore, the ceiling condition on a hot day is also taken into account.

This condition appears suitable as a design case for dedicated electric compressors which should pressurize the cabin using the most rarefied air within the aircraft envelope. This may represent a design condition for the system. The Table V shows the detailed inputs which are in line with those defined for model calibration. The temperatures and pressures of the air in the various components of the ACP are shown in Fig. 14-Fig. 17.

TABLE IV
GENERAL INPUT OF THE E-ECS MODEL FOR THE B787 DREAMLINER

Global input	Unit of measure	Value
Number of passenger	-	280
Number of crew members	-	10
Cruise Mach	-	0.85
Passenger window area	m^2	0.1269
Cockpit window area	m^2	4
Fuselage length	m	62.8
Fuselage radius	m	2.88
Flag passenger monitor	-	yes
Thickness of the outer skin of the fuselage	m	0.002
Thermal conductivity of the outer skin of the fuselage	W/(m K)	0.3
Thickness of the insulating layer of the fuselage	m	0.06
Thermal conductivity of the insulating layer of the fuselage	W/(m K)	0.04
Thickness of the decorative layer of the fuselage	m	0.005
Thermal conductivity of the fuselage decorative layer	W/(m K)	0.3
Wheel number of the ACM	-	2
Flag ACP subfreezing	-	yes
Minimum cabin pressure	bar	0.8127
Minimum air flow required per passenger	kg/s	0.0042

TABLE V
DETAIL INPUT OF THE E-ECS MODEL FOR THE B787 DREAMLINER

Detail input	Unit of measure	hot day ISA+25 (ground)	cold day ISA-35 (ground)	cold day ISA -20 (climb)	hot day ISA+20 (ceiling)
Isentropic efficiency of the ACM compressor	-	0.77	0.7	0.75	0.75
Isentropic efficiency of the ACM turbine	-	0.8	0.7	0.75	0.75
Mechanical efficiency of the ACM	-	0.98	0.98	0.98	0.98
Fan Efficiency	-	0.68	0.68	0.68	0.68
Mechanical efficiency of the fan	-	0.95	0.95	0.95	0.95
Electric Motor Fan efficiency	-	0.93	0.93	0.93	0.93
Pressure losses of the ram air	Pa	6000	6000	6000	6000
Pressure losses of the recirculation air	Pa	5000	5000	5000	5000
Cabin air temperature	°C	27	21	21	25

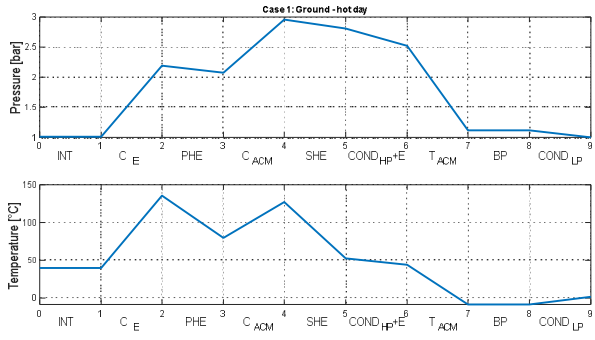

Fig. 14. E-ECS – ground hot day (Case 1) (where INT = intakes, C_E = E-ECS dedicated compressor, FCV = Flow Control Valve, PHE = Primary Heat Exchanger, C_{ACM} = ACM compressor, SHE = Secondary Heat Exchanger, COND HP = high pressure duct of the condenser, T_{ACM} = ACM turbine, BP = ByPass duct, COND LP = low pressure duct of the condenser)

When the aircraft is on the ground in hot day condition (Fig. 14), the ACM operates at maximum rpm to cool the cabin. In this condition, the differential temperature at the inlet and outlet of the heat exchangers (PHE and SHE) reach their maximum. In fact, the fan of the secondary air flow requires the maximum power. In this condition, it is not necessary to pressurize the cabin, therefore the ECS outlet pressure is equal to the external air pressure (no pressurization). As can be seen from Fig. 15, the CAU does not work to cool the cabin air in the cold day condition. In fact, the temperature of the air entering the CAU (PHE inlet – stage 2) is equal to that of the outlet (COND LP outlet – stage 9). In this condition, the secondary air flow is equal to zero (the temperature entering and leaving the heat exchangers is the same) and the dedicated compressor pressurizes the air to increase the air temperature. Fig. 16 shows the air pressure and temperature of the E-ECS during flight in cold day conditions. In that state, it is worth noting that the ACM is at idle speed. In fact, the variation in air pressure and temperature is minimal across the ACM. As in the previous condition, the secondary air flow is equal to zero and dedicated compressors pressurize the air to increase the pressure and temperature in order to pressurize and heat the cabin.

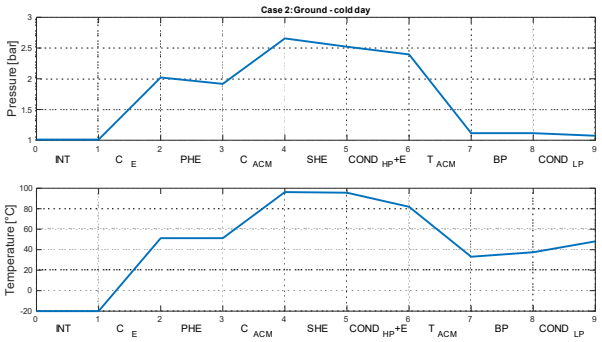

Fig. 15. E-ECS – ground cold day (Case 2) (where INT = intakes, C_E = E-ECS dedicated compressor, FCV = Flow Control Valve, PHE = Primary Heat Exchanger, C_{ACM} = ACM compressor, SHE = Secondary Heat Exchanger, COND HP = high pressure duct of the condenser, T_{ACM} = ACM turbine, BP = ByPass duct, COND LP = low pressure duct of the condenser)

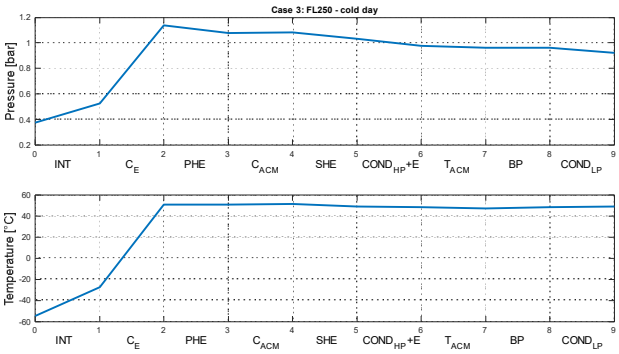

Fig. 16. E-ECS – FL250 cold day (Case 3) (where INT = intakes, C_E = E-ECS dedicated compressor, FCV = Flow Control Valve, PHE = Primary Heat Exchanger, C_{ACM} = ACM compressor, SHE = Secondary Heat Exchanger, COND HP = high pressure duct of the condenser, T_{ACM} = ACM turbine, BP = ByPass duct, COND LP = low pressure duct of the condenser)

Fig. 17 shows the E-ECS at ceiling and in hot day conditions. The air cycle machine is at idle speed, but in this condition, the secondary air flow is not zero (the temperature at the inlet and outlet of the heat exchangers is different). Due to the high pressurization demand (ceiling condition), the air temperature is too high to be distributed directly in the cabin. Therefore, it is necessary to reduce the air temperature using heat exchangers.

Comparing the results of E-ECS with those of conventional ECS, the following observations can be made:

- For the E-ECS, the compressed air - necessary to supply the ACP - reaches temperature between 50 and 155 °C depending on the operating conditions. These values are achieved without any heat exchanger. Typically, for conventional ECS, the temperature from the bleed air system is close to 200°C after passing through the pre-cooler. At the same flow rate required, the E-ECS requires less pneumatic power;
- A similar behavior is observed for the pressure of the supplied air. The dedicated compressors and air intake of the E-ECS compress the air at 1.1 to 2.2 bar depending on the conditions considered. Conventional ECS requires a higher pressure ranging from 1.9 to 2.7 bar. Moreover, also to account for one engine inoperative conditions, the bleed air system provides pneumatic power at pressures above 3 bar;
- During cruise, the E-ECS directly supplies hot air to the cabin by regulating its temperature mainly with PHE and SHE and reducing the load on the ACM. In contrast, the conventional ECS must reduce the hot air temperature from the bleed system by mixing it with the cold air supplied by the ACM.

In Table VI the flow rate required to the single ACP for each design condition is provided. It is worth noting that the most demanding phase considering this parameter is the hot ground condition. Finally, considering the pressure, flow rate, and efficiency of the dedicated compressor, it is possible to estimate the power required by the electric motor that drives the compressor.

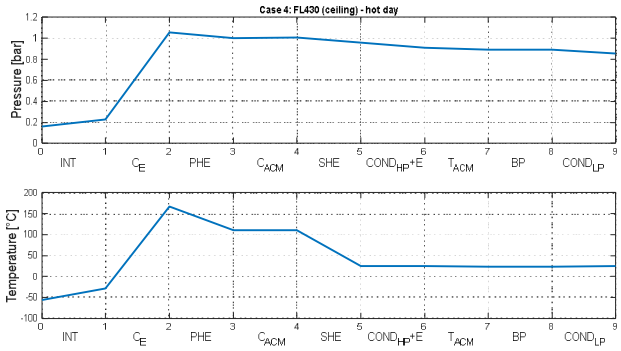

Fig. 17. E-ECS – FL430 hot day (Case 4) (where INT = intakes, C_E = E-ECS dedicated compressor, FCV = Flow Control Valve, PHE = Primary Heat Exchanger, C_{ACM} = ACM compressor, SHE = Secondary Heat Exchanger, COND HP = high pressure duct of the condenser, T_{ACM} = ACM turbine, BP = ByPass duct, COND LP = low pressure duct of the condenser)

TABLE VI
AIR FLOW RATE OF THE SINGLE AIR CONDITIONING PACK

Conditions	ACP Air flow rate [kg/s]
Ground Hot Day (Case 1)	0.925
Ground Cold Day (Case 2)	0.785
FL250 Cold Day (Case 3)	0.484
FL430 Hot Day (Case 4)	0.444

This is an important parameter since, for this architecture, it is the only reference available to validate the model. The model predicts a maximum compressor power of 71.7 kW in line with the reference value of 67.1-74.6 kW [36].

IV. Conclusion

This paper presented a simplified mathematical model for the preliminary design of the environmental control system. The model can be applied to several conventional ECS configurations, such as the two-wheel, three-wheel and four-wheel ACP, commonly employed in today's commercial aircraft. The model is also capable of designing the most advanced E-ECS and analyzing its performance. After a fairly simple calibration activities, mainly necessary to verify the performance of some components, the model was successfully applied to an aircraft belonging to another category and using the advanced E-ECS. Another important result was the opportunity to investigate the different behavior of conventional and electrified ECS. The results also confirmed the greater efficiency of the E-ECS due to two main technical characteristics:

- The E-ECS is supplied by dedicated compressors that produce the exact amount of pneumatic power required. While the conventional bleed system usually produces more power than required;
- During cruise, the most extensive phase for a commercial aircraft, dedicated compressors deliver air nearly compatible with cabin needs by bypassing the ACM. Conventional ECS must use the ACM to cool the air before it enters the cabin.

The main heat loads of the aircraft have been considered, but the modular structure of the model has allowed to add additional heat loads which could come from other components/systems of the aircraft such as the novel propulsion system (e.g., hybrid electric propulsion) which are not investigated here. Furthermore, the model could be further improved by modelling the reheater and other small components such as valves and pipes.

Acknowledgements

The research presented in this paper has been performed in the framework of the HERA project (Hybrid Electric Regional Aircraft) and has received funding from the European Union Horizon Clean Aviation Programme under grant agreement n◦ 101102007. The authors would like to thank Guido Pavan for his valuable help and advice.

References

[1] M. J. Cronin, All-Electric vs Conventional Aircraft: The Production/Operational Aspects, *Journal of Aircraft,* vol. 20, no. 6, pp. 481-486, 1983.

[2] I. Moir and A. Seabridge, *Aircraft Systems: Mechanical, electrical, and avionics subsystems integration*, Third ed., England: John Wiley & Sons, 2011.

[3] P. Della Vecchia, L. Stingo, F. Nicolosi, A. De Marco, G. Cerino, P. D. Ciampa, P. S. Prakasha, M. Fioriti, M. Zhang, A. Mirzoyan, B. Aigner and D. Charbonnier, Advanced turboprop multidisciplinary design and optimization within AGILE project, in *2018 Aviation Technology, Integration, and Operations Conference*, Atlanta, Georgia, 2018.

[4] L. Faleiro, J. Herzog, B. Schievelbusch and T. & Seung, Integrated equipment systems for a more electric aircraft-hydraulics and pneumatics, in *Proceedings of 24th International Congress of the Aeronautical Sciences*, 2004.

[5] R. I. Jones, The more electric aircraft—assessing the benefits, *Proceedings of the Institution of Mechanical Engineers, Part G: Journal of Aerospace Engineering,* vol. 216, no. 5, pp. 259-269, 2002.

[6] M. Fioriti, L. Boggero, S. Corpino, P. S. Prakasha, P. D. Ciampa and B. Nagel, The Effect of Sub-systems Design Parameters on Preliminary Aircraft Design in a Multidisciplinary Design Environment, *Transportation Research Procedia,* vol. 29, pp. 135-145, 2018.

[7] J. Kurzke, Gas turbine cycle design methodology: a comparison of parameter variation with numerical optimization, *Journal of engineering for gas turbines and power,* vol. 121, no. 1, pp. 6-11, 1999.

[8] L. Lupelli and T. Geis, *A study on the integration of the IP Power Offtake system within the Trent 1000 turbofan engine*. Master Thesis., 2012.

[9] M. Sinnet, 787 No-Bleed Systems: Saving Fuel and Enhancing Operational Efficiencies, *Aero Quarterly QTR_04 | 07,* pp. 06-11, 2007.

[10] Lisovin, I., Ekimov, S., Ismagilov, F., Vavilov, V., Gusakov, D., Bekuzin, V., Miniyarov, A., Development of a 250 kW Electric Power Generation System for a More Electric Aircraft, (2021) *International Review of Electrical Engineering (IREE)*, 16 (4), pp. 316-327. doi: https://doi.org/10.15866/iree.v16i4.19410

[11] P. Wheeler and S. Bozhko, The More Electric Aircraft: Technology and challenges, *IEEE Electrification Magazine,* vol. 2, pp. 6-12, 2014.

[12] Ismagilov, F., Zherebtsov, A., Vavilov, V., Sayakhov, I., Design and Experimental Investigation of BLDC Motor for Aircraft Electromechanical Actuator, (2020) *International Review of Aerospace Engineering (IREASE),* 13 (1), pp. 10-15. doi: https://doi.org/10.15866/irease.v13i1.17849

[13] A. Abdel-Hafez, Power Generation and Distribution System for a

More Electric Aircraft - A review, Dr. Ramesh Agarwal, ISBN: 978-953-51-0150-5, *Intech*, 2012, pp. 289-308.
[14] D. van den Bossche, The A380 fligh control electrohydrostatic actautors, achievements and lessons learnt, in *ICAS*, Hamburg, 2006.
[15] I. Berlowitz, All/More Electric Aircraft Engine & Airframe Systems Implementation, in *The 9th Israeli Symposium on Jet Engines and Gas Turbines*, 2010.
[16] I. Jennions, F. Ali, M. Esperon Miguez and I. Camacho Escobar, Simulation of an Aircraft Environmental Control System, *Applied Thermal Engineering,* vol. 172, no. 114925, pp. 1-36, 2020.
[17] S. H. Chowdhury, F. Ali and I. K. Jennions, A review of aircraft environmental control system simulation and diagnostics, *Proceedings of the Institution of Mechanical Engineers, Part G: Journal of Aerospace Engineering,* pp. 1-15, 2023.
[18] D. P. Linares, *Modeling and Simulation of an Aircraft Environmental Control System*, Doctoral dissertation, École Polytechnique de Montréal, 2016.
[19] D. Bender, Exergy-Based Analysis of Aircraft Environmental Control Systems – Integration into Model-Based Design and Potential for Aircraft System Evaluation, in *ECOS 2016 - The 29th International Conference on Efficiency, Cost, Optimization, Simulation and Environmental Impact of Energy Systems*, 2016.
[20] M. Kwiatkowski, *Simulation of Components from the Environmental Control System,* Project report - HAW Hamburg, Hamburg, 2006.
[21] Orozco, W., Acuña, N., Orjuela Abril, S., CFD Study of the Heat Exchange Process in an Energy Recovery System Applied to Low Displacement Diesel Engines, (2020) *International Review on Modelling and Simulations (IREMOS)*, 13 (4), pp. 243-251. doi:https://doi.org/10.15866/iremos.v13i4.18605
[22] J. Vargas and A. Bejan, Thermodynamic optimization of finned crossflow heat exchangers for aircraft environmental control systems, *International Journal of Heat and Fluid Flow,* vol. 22, no. 6, pp. 657-665, 2001.
[23] Y. Yang, S. Chen, C. Sheng, H. Xie, G. Luo and Y. Hou, Study on coupling performance of turbo-cooler in aircraft environmental control system, *Energy,* vol. 224, no. 120029, pp. 1-13, 2021.
[24] Alvarenga, M., Andrade, C., Zaparoli, E., A Thermodynamic Analysis of Three and Four-Wheel Air Cycle Machines for Aeronautical Applications, (2015) *International Review of Mechanical Engineering (IREME)*, 9 (2), pp. 190-200. doi: https://doi.org/10.15866/ireme.v9i2.5543
[25] T. Planès, S. Delbecq, V. Pommier-Budinger and E. Bénard, Modeling and Design Optimization of an Electric Environmental Control System for Commercial Passenger Aircraft, *Aerospace,* vol. 10, no. 3, p. 260, 2023.
[26] L. Patricelli, *Innovative solutions for the thermal control of aeronautic vehicles*, Master thesis, 2013.
[27] Y. Han, C. Yang, X. Zhang and X. Yuan, Influences of Different Architectures on the Thermodynamic Performance and Network Structure of Aircraft Environmental Control System, *Entropy,* vol. 23, no. 7, 2021.
[28] Z. Duan, H. Sun, C. Wu and H. Hu, Multi-objective optimization of the aircraft environment control system based on component-level parameter decomposition, *Energy,* vol. 245, no. 123330, pp. 1-15, 2022.
[29] R. Vega Diaz, *Analysis of an electric environmental control system to reduce the energy consumption of fixed-wing and rotary-wing aircraft*, Master thesis, Cranfield, 2011.
[30] ASHRAE, Aircraft, in *Heating, ventilating, and air conditioning: analysis and design*, American Society of Heating, Refrigerating and Air-Conditioning Engineers, Inc., 2015.
[31] D. W. Green and R. H. Perry, *Perry's chemical engineers'handbook*, vol. 2, McGraw-Hill, 2008, pp. 2-155.
[32] SAE-AIR-1168/3, *Aerothermodynamic Systems Engineering and Design*, SAE aerospace, 2011.
[33] F. P. Incropera and D. P. DeWitt, F*undamentals of Heat and Mass Transfer*, 3rd ed., New York: Wiley, 1990, pp. 658-660.
[34] SAE-AIR-1168/6, *Characteristics of Equipment Components, Equipment Cooling System Design, and Temperature Control System Design*, SAE International, 2004.
[35] Liebherr-Aerospace, *A319/A320/A321 Environmental Control System - Familiarization Training*, Liebherr-Aerospace, 2004.
[36] M. A. Dornheim, Electric cabin, *Aviation week and space technology,* pp. 47-49, 28 March 2005.

Authors' information

Department of Mechanical and Aerospace Engineering, c.so Einaudi 40, Turin, Italy.

Marco Fioriti Turin, Italy. 8th July 1980. Education: in 2010, PhD degree in Aerospace Engineering at Politecnico di Torino. The title of the thesis was "Innovative solutions for light, ultralight and unmanned aircraft". Work experience: since 2010, he has been a researcher and lecturer in aerospace systems design at Politecnico di Torino, focusing his research on aircraft conceptual design, on-board systems preliminary design, MDO methodologies, Reliability, Availability, Maintainability, Safety disciplines and aircraft Life Cycle Cost / Life Cycle Assessment estimation algorithms. He has contributed to several national and European research programs (Clean sky SAGE, Agile H2020, Clean Sky 2 IRON, AGILE 4.0, Clean Aviation HERA, Colossus) and he is the author of several scientific articles and congress proceedings. He setup several collaborations with LEONARDO Aircraft Division and LEONARDO Labs. He is a member of the American Institute of Aeronautics and Astronautics – Electrified Aircraft Technology TC.

Flavio Di Fede Syracuse, Italy. 9th October 1994. Education: in 2019, a MSc degree in Aerospace Engineering at Politecnico di Torino, Italy. Work experience: since 2019, he specialized in aircraft on-board system design with a research fellowship at Politecnico di Torino from 11/2019 to 04/2022. The research project focused on the design and integration of new on-board system architectures. His main tasks cover managing innovative aircraft architecture technical activities, mainly in on-board system design for hybrid-electric regional aircraft.